




Microstructure characterization and tensile properties of a Ni-containing TiAl-based alloy with heat treatment

Jian-Chao Han, Shu-Long Xiao, Jing Tian,
Yu-Yong Chen* , Li-Juan Xu, Xiao-Peng Wang,
Yi Jia, Shou-Zhen Cao

Received: 30 May 2015 / Revised: 18 August 2015 / Accepted: 24 September 2015 / Published online: 27 October 2015
© The Nonferrous Metals Society of China and Springer-Verlag Berlin Heidelberg 2015

Abstract The effects of Ni addition on solidification microstructure and tensile properties of Ti-48Al-2Cr-2Nb alloy were investigated using differential scanning calorimetry (DSC), X-ray diffraction (XRD), scanning electron microscopy (SEM) equipped with energy-dispersive spectroscope (EDS) and transmission electron microscopy (TEM). Results show that with 3 at% Ni addition, the as-cast microstructure is mainly composed of fine lamellar colonies ($\sim 50 \mu\text{m}$), γ grains and Ni-riched τ_3 phase. After heat treatment at 1380 °C, the Ni-containing alloy is characterized by fine fully lamellar microstructure ($\sim 90 \mu\text{m}$). The heat-treated Ni-containing specimen exhibits superior room temperature tensile properties than other specimens. The tensile properties are discussed in light of the microstructure evolution and role of Ni-riched τ_3 phase.

Keywords TiAl-based intermetallics; Solidification microstructure; Heat treatment; Phase transformation; Tensile properties

1 Introduction

The advantages of TiAl-based alloys, such as low density, specific modules, specific high temperature strength and excellent creep property, make them the most attractive candidate materials for aerospace application [1–3]. Because of high material cost and limited formability, TiAl-based alloys tend to favor near-net shape processes such as casting. However, the formation of coarse-grained microstructure during solidification [4] and significant chemical inhomogeneity [5] of TiAl-based castings further deteriorates the initial low ductility at ambient temperature. This severely limits their further developments [6]. Accordingly, much attention has been focused on obtaining an understanding of the structure–property relationship in these alloys and improving their ductility.

TiAl alloys with fine fully lamellar (FFL) colonies are demonstrated to exhibit the prior combination of mechanical properties [7]. The main method used for this desired microstructure is the thermomechanical processing such as extrusion or forging at elevated temperature plus heat treatment [8] and minor alloying, such as B [9]. However, the first method involves mechanical processing at high temperature and even in vacuum and therefore induces significant difficulty in experimentation and considerable cost in production. On the other hand, B alloying would bring brittle borides into the base alloy. Studies by Hu [10] demonstrated that the tensile properties of B-containing TiAl alloys severely relied on the size of borides and the ductility may be deteriorated inversely by the large-sized borides. To simplify the processing route and avoid the brittle reinforcement phase, researchers tended to favor heat treatment only for the FFL microstructure [11, 12]. However, the reported heat treatments are always multi-step or cycle heat treatment, which still appear to be

J.-C. Han, S.-L. Xiao, J. Tian, Y.-Y. Chen*, L.-J. Xu,
X.-P. Wang, Y. Jia, S.-Z. Cao
School of Materials Science and Engineering, Harbin Institute of
Technology, Harbin 150001, China
e-mail: yychen@hit.edu.cn

J.-C. Han, S.-L. Xiao, Y.-Y. Chen, X.-P. Wang, Y. Jia,
S.-Z. Cao
National Key Laboratory of Science and Technology on
Precision Heat Processing of Metals, Harbin Institute of
Technology, Harbin 150001, China

Y.-Y. Chen
State Key Laboratory of Advanced Welding and Joining, Harbin
Institute of Technology, Harbin 150001, China

complicated for engineering application. So there remains requirement for simple method to obtain FFL microstructure, as well as corresponding mechanical properties.

As a common element from the iron group, Ni has been confirmed to be a potential alloying element as a minor constituent in TiAl [13]. The ductility [14] and hot workability [15] of TiAl-based alloys have been improved by moderate Ni addition (0.5 at%–1.0 at%). It was also found that Ni can enlarge the γ phase zone in Ti–Al phase diagram and is beneficial to stabilize γ phase [16]. In addition, with adequate Ni addition, the solidification path of common TiAl-based alloys would be transformed by inducing a novel phase [17]. While the solidification microstructure of Ni-containing conventional TiAl-based alloy and the influence of simple single-step heat treatment are still unclear, the objective of the present work was to investigate the microstructure characterization and tensile properties of Ni-containing TiAl-based alloy with single-step heat treatment. The solidification microstructure and phase transformation during heat treatment were discussed in detail.

2 Experimental

Alloys of nominal compositions of Ti-48Al-2Cr-2Nb-(0, 3) Ni (T4822 and T4822-Ni thereafter; at%) were chosen for the investigation. The parent materials used in this study contained Ti bar (>99.99 wt%), pure Al (>99.99 wt%), master alloy Al-Nb (52.59 wt%), pure Cr (>99.99 wt%) and Ni powders (>99.99 wt%). The raw materials were blended and then melted in an induction skull melting furnace (ISM) under an Ar atmosphere (pressure of ~ 50 kPa). In order to ensure the sufficient uniformity of composition and microstructure, thermal insulation and electromagnetic stirring were conducted for 300 s in the melt condition. The melt was poured into a 500 °C preheated metal mold forming cylindrical ingot with size of $\Phi 50$ mm \times 60 mm. Chemical compositions of the ingots were measured by X-ray fluorescence (XRF, AXIOS-PW4400), as listed in Table 1.

Differential scanning calorimetry (DSC, NETZSCH STA 449F3) was used to analyze the thermal events in the T4822-Ni alloy during heating to 1400 °C at 20 °C \cdot min $^{-1}$ in flowing high-purity argon. Samples for heat treatment,

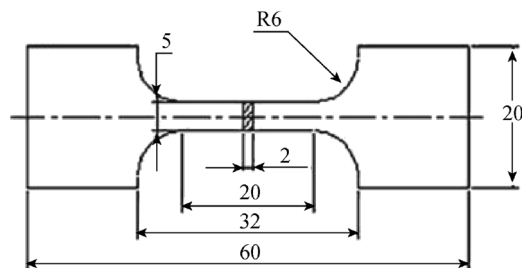


Fig. 1 Dimensioned schematic of RT tensile specimen (unit: mm)

microstructure observation and tensile test were cut by electric discharging from the ingot. Subsequent heat treatment was carried out in a tube furnace under an Ar atmosphere (pressure of 100 kPa) at 1380 °C for 30 min, followed by furnace cooling (T4822-HT and T4822-Ni-HT thereafter). After heat treatment, the oxidized surface layer was carefully removed from the specimens before proceeding further. The phase constituents and microstructure of the samples were examined by X-ray diffraction (XRD, Rigaku D/MAX RB, Cu target), scanning electron microscopy (SEM, FEI Quanta 200F) equipped with energy-dispersive spectroscopy (EDS) and transmission electron microscopy (TEM, Tecnai G2 F30). The average grain size was estimated by a line intercept technique on at least ten SEM images. The lamellae spacing (λ) was determined using several bright-field TEM images in the “edge-on” condition. Flat tensile specimens with dimensions shown in Fig. 1 were performed on Instron 5500R testing machine at room temperature (RT), driven at crosshead speed of 0.5 mm \cdot min $^{-1}$. At least three tests were performed under each condition, and the average values were reported. Fracture surfaces were observed to understand fracture mechanisms.

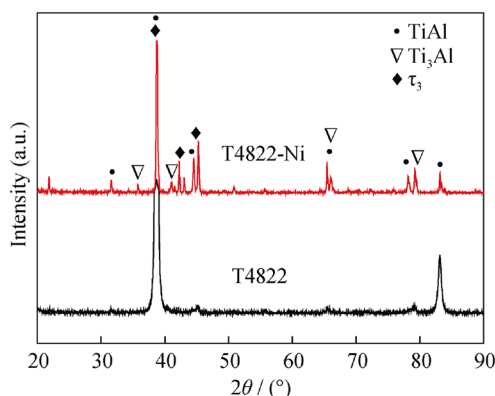


Fig. 2 XRD patterns of T4822 and T4822-Ni alloys

Table 1 Measured chemical compositions of Ti-48Al-2Cr-2Nb alloys with Ni addition (wt%)

Alloys	Al	Cr	Nb	Ni	O	N	Ti
T4822	32.75	2.65	4.78	–	0.07	0.01	Bal.
T4822-Ni	32.89	2.58	4.97	4.41	0.08	0.01	Bal.

3 Results and discussion

3.1 As-cast microstructure

Figure 2 shows the XRD patterns of as-cast T4822 and T4822-Ni alloys. It is shown that the matrix T4822 alloy consists of dominant γ and α_2 phases. With 3 at% Ni

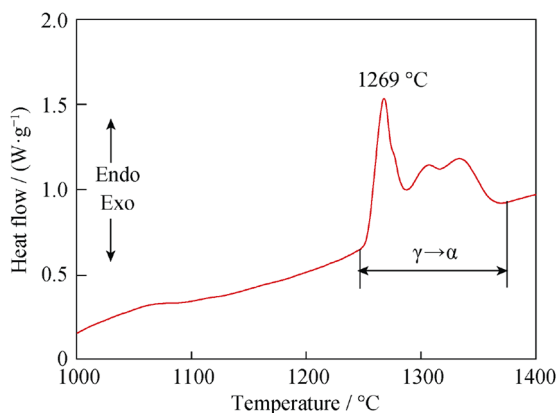


Fig. 3 DSC curve of T4822-Ni alloy during heating to 1400 °C at 20 °C·min⁻¹ in flowing high-purity argon

addition, τ_3 phase is detected other than γ and α_2 phases. It is a hexagonal-structured intermetallic phase with the approximate composition of Al_3NiTi_2 . The formation of Al_3NiTi_2 phase (known as τ_3 phase) in TiAl-based alloys was reported in other researches as well [17, 18]. It is a metastable ternary intermetallic phase, arising from the corresponding solidification process of Ti–Al–Ni [19].

The DSC curve obtained from T4822-Ni alloy is shown in Fig. 3. The broad endothermic peak detected on the DSC curve for the alloy corresponds to $\gamma \rightarrow \alpha$ transformation. The endothermic reaction at 1269 °C will be discussed later.

Figure 4 shows the microstructures of as-cast T4822 and T4822-Ni alloys. It is obvious to observe from Fig. 4a, b that the predominant microstructure of the matrix alloy (T4822) is near fully lamellar (NFL). It consists primarily of $(\alpha_2 + \gamma)$ lamellar colonies with nonlinear grain boundary. Evident dendrite microstructure with dark and bright contrasts can be clearly observed in Fig. 4a. These interdendritic regions (dark contrast) are named as Al segregation and demonstrated to be enriched with Al element, according to the EDS data (Table 2). Bright ridges can be seen in the dendrites, which appear to be the residual β phase under nonequilibrium solidification. Those areas are

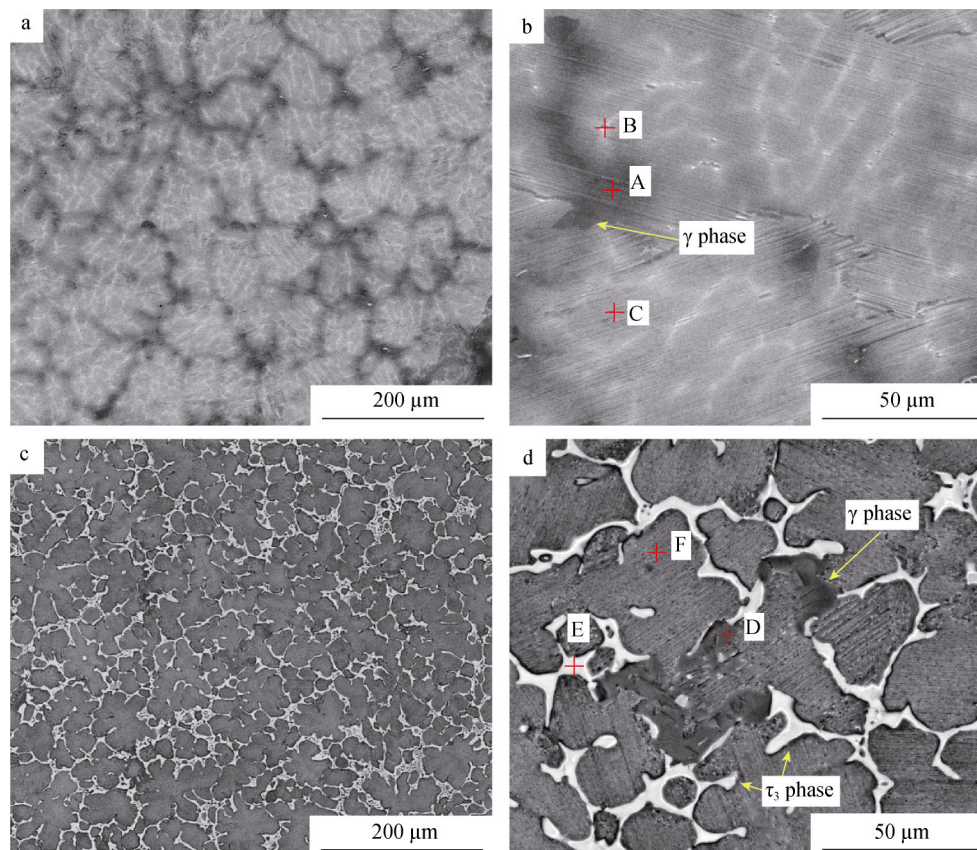


Fig. 4 SEM images of **a, b** T4822 alloy and **c, d** T4822-Ni alloy

Table 2 Chemical compositions of Spots A–F shown in Fig. 4b, d (at%)

Elements	T4822			T4822-Ni		
	A	B	C	E	D	F
Ti	44.88 ± 0.58	48.05 ± 0.34	47.83 ± 0.28	31.68 ± 0.85	45.18 ± 0.35	48.27 ± 0.65
Al	49.97 ± 0.55	45.70 ± 0.52	48.12 ± 0.28	46.37 ± 0.75	49.21 ± 0.48	47.12 ± 0.68
Cr	3.28 ± 0.33	3.44 ± 0.13	2.07 ± 0.12	4.76 ± 0.33	1.92 ± 0.13	1.58 ± 0.23
Nb	1.87 ± 0.13	2.81 ± 0.35	1.98 ± 0.03	1.67 ± 0.16	2.21 ± 0.12	2.27 ± 0.31
Ni	–	–	–	15.52 ± 0.16	1.48 ± 0.05	0.76 ± 0.12

enriched with beta-stabilizing elements, here are the Cr and Nb. It is noticeable that the enrichment of Cr occurs in both Al segregation areas and the residual β phase, while Nb gathers only in the residual β phase. This can be mainly attributed to the distinction of partition coefficient (k) in α and β phases [20]. Measured by the linear intercept method, the grain size of the as-cast T4822 alloy is about 600–1000 μm . Figure 4c, d shows the microstructures of T4822-Ni alloy. As can be seen, the microstructure is mainly composed of lamellar colonies, γ grains and an increased amount of bright ridges. As analyzed by EDS, these ridges are enriched in Ni element, with the approximate atom ratio of Al:Ni:Ti = 3:1:2. These Ni-riched phases mainly distribute along the lamellar colony boundaries, accompanied by dark γ grains. Meanwhile, the lamellar colonies are equiaxed and refined, with an average colony size of $\sim 50 \mu\text{m}$.

As shown in Fig. 4, with Ni addition the RT phase composition of T4822 transforms from $\alpha_2 + \gamma + \beta$ (trace) to $\alpha_2 + \gamma + \tau_3$. This can be mainly attributed to the change of solidification path. According to Ti–Al–Ni ternary phase diagram [17], the solidification path of the present Ni-containing alloy should proceed as follows, $L \rightarrow L + \beta \rightarrow L + \alpha \rightarrow L + \alpha + \tau_3 \rightarrow \alpha + \tau_3 \rightarrow$ lamellae ($\alpha_2 + \gamma$) + $\gamma + \tau_3$. It is noteworthy that τ_3 phase forms in the posterior stage of solidification, so it is reasonable for the distribution of τ_3 phase along the grain boundaries (Fig. 4d). It is noted that Ni content in γ phase is almost twice that in colony, indicating that the solid solution of Ni is higher in γ phase than in α_2 phase. Actually, the solubility of Ni in α_2 and γ phases do not appear to be an absolute value. According to Ref. [17], there is a quite low solubility of Ni in Ti_3Al compound, which is almost one-third that in γ phase. This can account for the partition phenomenon of Ni element in Fig. 4 and Table 2.

Figure 5 shows TEM images of as-cast T4822 and T4822-Ni alloys in the edge-on condition and corresponding selected area diffraction (SAD) pattern. From Fig. 5a, it can be got that the lamellae of T4822 are coarse. The average lamellae spacing is about 300 nm, and the γ lath is much larger than the α_2 lath. Figure 5b shows the

lamellar colony triple junction of the matrix T4822 alloy. As observed, the lamellae orientation between adjacent colonies is intersectant, and there exists many γ grains along the colony boundary, corresponding to Fig. 4b. In contrast, the Ni-containing alloy reveals a predominantly fine lamellar microstructure, as shown in Fig. 5c. The average lamellae spacing is about 200 nm, much thinner than that of T4822. Meanwhile, the width of γ and α_2 laths is almost equivalent, in contrast to that of T4822. As can be seen, the boundaries between lamellae are clear, similar to the matrix T4822 alloy. The bulk phase in Fig. 4d is further identified as Ni-riched τ_3 phase with hexagonal structure ($a = 5.0129 \text{ nm}$, $c = 8.1596 \text{ nm}$) by TEM (Fig. 5d). With the assistance of diffraction, no evidence of clear orientation relationship (OR) between τ_3 phase and surrounding matrix is found. As arrowed in Fig. 5d, there exist lots of dislocations in the base alloy and τ_3 grains, which are almost parallel to each other. As observed, the dislocations appear to favor matrix phase rather than bulk τ_3 grain, indicating that the dislocation is hard to activate or slip within the τ_3 phase.

3.2 Microstructure after heat treatment

Figure 6 shows the microstructure of T4822 and T4822-Ni alloys after heat treatment at 1380 $^\circ\text{C}$. The temperature and holding time of this heat treatment are referred from the published literature [21] and the DSC results (Fig. 3) in order to obtain fully lamellar (FL) microstructure and reduce element segregation. As can be clearly seen, the residual β phase is almost eliminated after heat treatment. However, the trace of Al segregation remains and the segregation degree is weakened compared to the as-cast microstructure (Fig. 4b). Meanwhile, the lamellae exhibit a slight coarsening, especially for the lamellar colony boundary. After heat treatment, the grain size of alloy increases slightly with an average value of 800 μm . For the Ni-containing alloy, the major influence of heat treatment is the elimination or decomposition of bright bulk τ_3 phase. The heat-treated microstructure consists of equiaxed fully lamellar colonies, without any trace of element segregation. Figure 7 reveals the grain size distribution of heat-

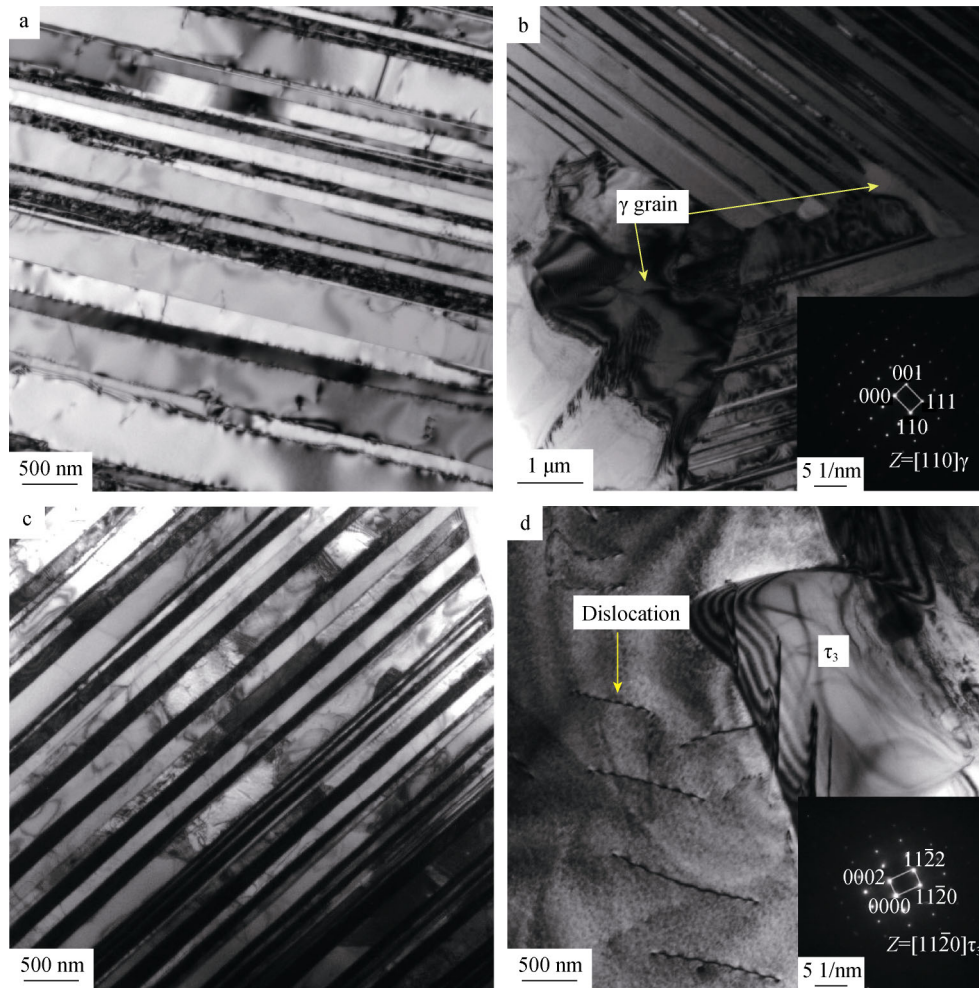


Fig. 5 TEM images of as-cast T4822 and T4822-Ni alloys and corresponding SAD pattern: **a, b** bright-field image of as-cast T4822 alloy; **c, d** bright-field image of as-cast T4822-Ni alloy. Insets in **b, d** showing corresponding SAD pattern

treated T4822-Ni alloy. Overall, the grain size is no larger than $180 \mu\text{m}$, with an average size of $90 \mu\text{m}$. And for half content of the heat-treated grains, the grain size ranges from 60 to $130 \mu\text{m}$. As can be seen, the grain size appears to be larger than that of as-cast T4822-Ni alloy, while it is still much smaller than that of as-cast and heat-treated T4822 alloys.

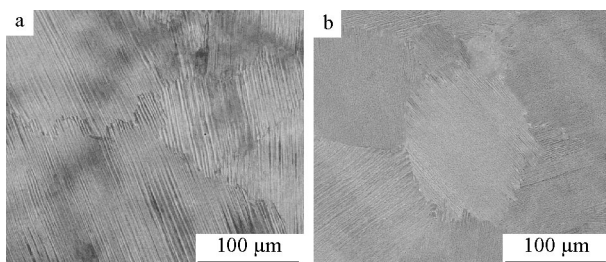


Fig. 6 SEM images of **a** T4822 alloy and **b** T4822-Ni alloy after heat treatment at $1380 \text{ }^\circ\text{C}$ for 30 min

Figure 8 shows TEM images of Ni-containing alloy after heat treatment. As can be seen in Fig. 8a, the lamellae spacing is equivalent to that of as-cast alloy, while the γ lath appears to be larger than the α_2 lath. The small bulk

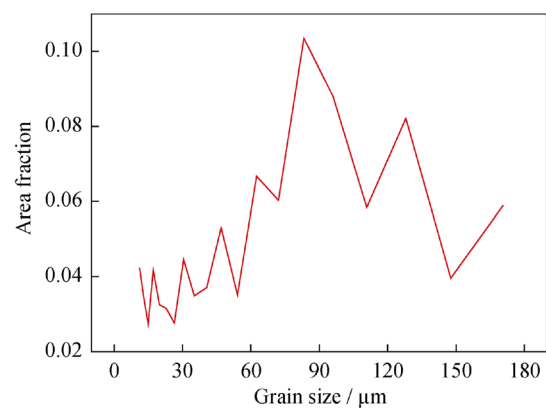


Fig. 7 Grain size distribution of heat-treated T4822-Ni alloy

phase between coarse γ laths is found, as arrowed in Fig. 8a. The corresponding diffraction SAD pattern reveals that these discontinuous particles are γ phase, with OR with α_2 lath as $[11\bar{2}0]\alpha_2//[1\bar{1}0]\gamma$ and $(0001)\alpha_2//(111)\gamma$ corresponding to the Blackburn OR [22]. Figure 8c, d shows the needlelike precipitations in the lamellae structure, which are identified as the Ni-riched τ_3 phase with $[0001]$ zone. The τ_3 phases exhibit great length/diameter ratio (~ 20), evidently different with the bulk τ_3 phase in the as-cast alloy (Fig. 5d). This indicates that the τ_3 phase is transformed during the heat treatment.

According to the Ti–Al binary phase diagram [23], the broad endothermic feature shown in Fig. 3 for T4822-Ni alloy indicates the endothermic reaction event, namely $\gamma \rightarrow \alpha$. The heat treatment temperature in the present work appears to be in the single α phase region. The endothermic reaction peaked at 1269 °C (Fig. 3) can be assumed to be reaction $\tau_3 + \gamma \rightarrow \alpha + L$, which occurs at ~ 1272 °C according to Schuster et al. [17]. As temperature increases,

more α phase would be transformed from γ phase, and this might enable more Ni-riched liquid formation until the τ_3 phase is consumed. So during the heat treatment at 1380 °C, the bulk τ_3 phase is eliminated according to the reaction $\tau_3 + \gamma \rightarrow \alpha + L$, and the equilibrium phases should be α phase (solid) and persistent liquid phase [18]. The chemical homogenization may occur during this process, which means that the Ni diffuses into α phase. Considering the normal Ar atmosphere (pressure of 100 kPa), the element evaporation during heat treatment can be ignored. Then during subsequent cooling, α phase should transform to $\alpha + \gamma$ phases and finally to the dual-phase colony. In light of the Al–Ti–Ni liquid projection diagram [17], τ_3 phase should re-precipitate according to the reaction $\alpha \rightarrow \alpha + \gamma + \text{secondary } \tau_3$. Therefore, the needle-like τ_3 phase in Fig. 8c, d should be the production of re-precipitation during heat treatment. As shown in Fig. 8, the needle-like τ_3 phases mainly distribute in a certain region rather than the whole specimen. This can be mainly

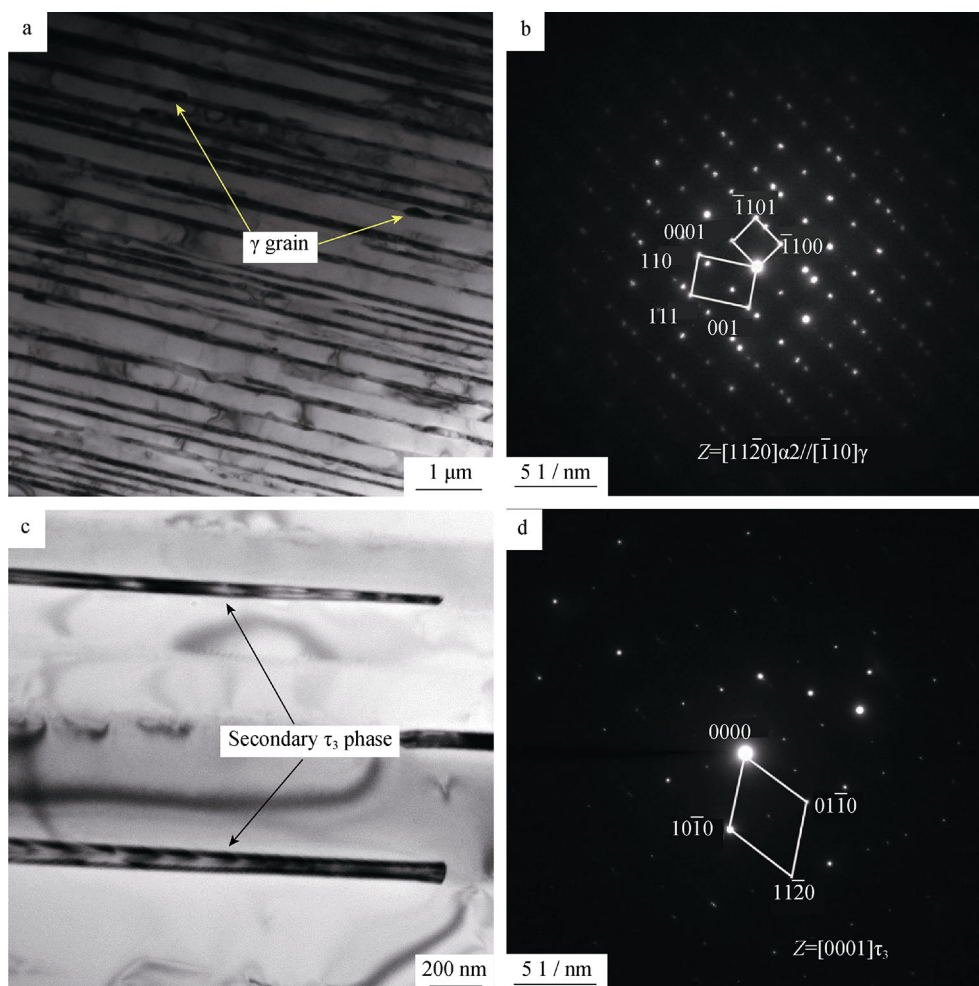


Fig. 8 TEM images of heat-treated T4822-Ni alloy and corresponding SAD pattern: **a** bright-field image of lamellar structure, **b** corresponding SAD pattern of γ particles and matrix shown in **a**, **c** bright-field image of secondary τ_3 phase and **d** corresponding SAD pattern

attributed to the initial distribution of bulk τ_3 phases along the grain boundary accompanied by γ grains (Fig. 4d). During heat treatment, the regenerated α phase and Ni-riched liquid remain and subsequently transform in the initial region. Therefore, the nonuniform distribution of the secondary needlelike τ_3 phase should be attributed to the incomplete homogenization of Ni element.

3.3 Tensile properties and fractography

The tensile properties of the as-cast and heat-treated T4822 and T4822-Ni alloys at RT are shown in Fig. 9. As shown, after heat treatment, T4822 and T4822-Ni alloys exhibit evident yield phenomenon, while the as-cast alloy undergoes an absolute elastic deformation to fracture. The tensile properties and microstructure features in the present work are summarized in Table 3. According to the stress–strain curves and corresponding test data, it can be obtained that the as-cast Ni-containing alloy exhibits the worst tensile property, though its microstructure seems to be refined. According to previous researches, the influence of Ni addition in γ -TiAl-based alloys on tensile properties appears to be controversial. A small addition of Ni addition (0.5 at%–1.0 at%) was reported to improve the ductility [14], while more addition was proved to be harmful for the ductility [24]. This may be attributed to the precipitation of Ni-riched τ_3 phase, corresponding to the deterioration

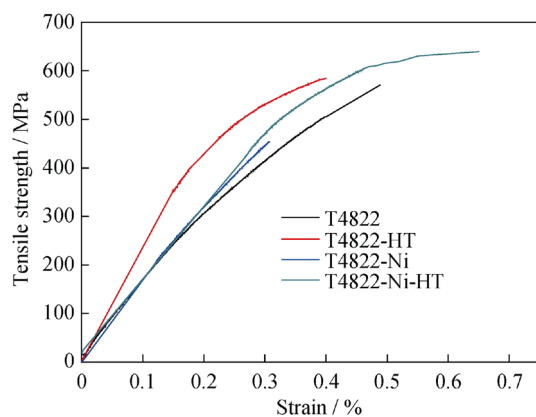


Fig. 9 Tensile stress–strain curves of as-cast and heat-treated T4822 and T4822-Ni alloys at RT

Table 3 Microstructure features and tensile properties at RT

Alloys	Microstructure	Grain size/ μm	λ/nm	YS/MPa	UTS/MPa	$\varepsilon_f/\%$
T4822	NFL	700 ± 100	300 ± 10	312 ± 10	570 ± 20	0.48 ± 0.05
T4822-HT	Coarse FL	800 ± 110	350 ± 15	360 ± 15	584 ± 15	0.40 ± 0.03
T4822-Ni	FL + γ + τ_3	50 ± 10	200 ± 8	–	453 ± 18	0.30 ± 0.04
T4822-Ni-HT	Fine FL	90 ± 15	190 ± 10	445 ± 18	640 ± 20	0.65 ± 0.08

effect of brittle B2 phase on RT tensile property. With hexagonal phase lattice, the Ni-riched τ_3 particles distribute in TiAl-based alloy as additional intermetallic phase. They can hardly provide additional slip system for plastic deformation, but work as brittle fracture source during strain loading. So this results in the deteriorative tensile properties of the as-cast Ni-containing alloy.

On the other side, the T4822 alloy shares the equivalent tensile strength and elongation to failure which appear to be unaffected by heat treatment (Table 3). On the contrary, the yield strength (YS) and ultimate strength (UTS) of heat-treated Ni-containing alloy are 445 and 640 MPa, respectively, with an elongation to failure (ε_f) of 0.65 %. The YS and UTS are 85 and 56 MPa greater than those of T4822-HT alloy. As illustrated above, the T4822-Ni alloy exhibits finer lamellar colonies and lamellae spacing after heat treatment (Table 3). According to the classic Hall–Petch equation:

$$\sigma_s = \sigma_0 + kd^{-1/2} \quad (1)$$

where σ_s is yield stress, σ_0 and k are material constants, and d is the mean grain size. It is understood that d is the only structural variable that determines the yield stress. Generally in previous works, the strength data of lamellar TiAl alloys were presented in terms of the Hall–Petch relation [21]. So in the present work, the fine colony size and lamellae spacing should account for the strengthening and ductility of heat-treated Ni-containing alloy. According to the result in Ref. [10], T4822-1B alloy with similar grain size exhibits lower YS (345 MPa), but higher ε_f (1.4 %) than those of T4822-Ni-HT alloy in the present work. This may be attributed to the re-precipitation of needlelike τ_3 phase within the lamellar structure during heat treatment. As observed in Fig. 5b, d, there exist lots of dislocations within γ phase while little in τ_3 phase. This indicates that the dislocation appears to be hard to activate or slip within τ_3 phase. During deformation, these τ_3 particles may act as pins for the dislocation slip. This may lead to the dislocation pileup, contributing to the strengthening of the studied alloy. On the other side, this high density of dislocation may result in partial stress concentration, leading to the untimely fracture during strain loading.

Figure 10 shows the fracture surfaces of the studied alloys tested at RT. The as-cast T4822 alloy presents typical trans-

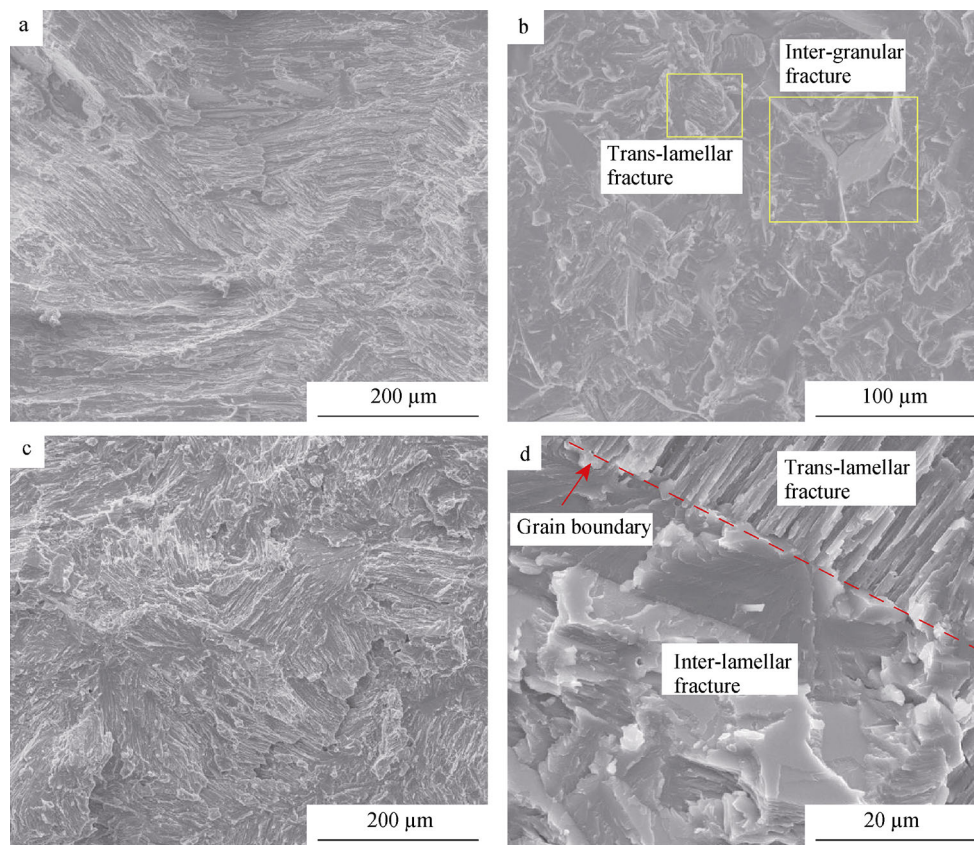


Fig. 10 SEM images of fracture surface of tensile samples of as-cast and heat-treated T4822 and T4822-Ni alloys at RT: **a** as-cast T4822, **b** as-cast T4822-Ni, **c** T4822-Ni-HT and **d** magnified image of **c**

lamellar fracture mode with great fracture planes (Fig. 10a). However, the fracture surface of the as-cast T4822-Ni alloy has typical inter-granular and trans-lamellar fracture modes, as marked in Fig. 10b. This may be attributed to the distribution of brittle τ_3 phase along the grain boundaries. During the tensile testing, these second intermetallic particles can activate the nucleation of crack, leading to the crack propagation through themselves [24]. So this may account for the rapid failure and terrible tensile behavior. On the contrary, the heat-treated Ni-containing alloy presents both the trans-lamellar and inter-lamellar fracture modes, similar to the general lamellar TiAl alloys (Fig. 10c). From the high magnification image (Fig. 10d), the clear transformation between trans-lamellar and inter-lamellar fracture modes can be observed. It is noteworthy that the intact grain boundary connecting the two different fracture planes indicates that for the T4822-Ni-HT alloy, grain boundary does not appear to be the prior fracture location.

4 Conclusion

In this study, microstructure characterization and tensile properties of a Ni-containing TiAl-based alloy with heat

treatment were investigated in detail. Experimental results show that, with 3 at% Ni addition, the as-cast microstructure is mainly composed of fine lamellar colonies ($\sim 50 \mu\text{m}$), γ grains and Ni-riched τ_3 phase. The bulk τ_3 phase mainly distributes along the lamellar colony boundaries, accompanied by bulk γ grains. After heat treatment at $1380 \text{ }^\circ\text{C}$, the matrix alloy shows little microstructure variation, while the Ni-containing alloy exhibits fine fully lamellar microstructure with average grain size of $90 \mu\text{m}$. During heat treatment, the bulk τ_3 phase is re-melted through $\tau_3 + \gamma \rightarrow \alpha + \text{L}$ reaction and re-precipitates with subsequent cooling. The fine secondary needlelike τ_3 phases mainly distribute between the lamellae in certain regions, with large length/diameter ratio (~ 20). The heat-treated Ni-containing specimen exhibits superior tensile properties (YS of 445 MPa and ϵ_f of 0.65 %) than other specimens. The elimination of bulk τ_3 phase, refined lamellar colonies and lamellae spacing can account for the strengthening of current heat-treated T4822-Ni specimen, as well as the ductility.

Acknowledgments This study was financially supported by the National Natural Science Foundation of China (Nos. 51001040, 51371064 and 51504075) and the Shanghai Aerospace Science and Technology Innovation Fund (No. SAST201428).

References

- [1] Kim YW. Microstructural evolution and mechanical properties of a forged gamma titanium aluminide alloy. *Acta Metall Mater.* 1992;40(6):1121.
- [2] Clemens H, Kestler H. Processing and applications of intermetallic γ -TiAl-based alloys. *Adv Eng Mater.* 2000;2(9):551.
- [3] Xu ML, Yang XK, Zhang YJ, Xia SB, Dong P, Yang GT. Microstructure and formation mechanism of SHS joining between C_p/Al composites and TiAl intermetallic with Al–Ni–CuO interlayer. *Rare Met.* 2015;34(1):17.
- [4] Liu Y, Hu R, Kou HC, Wang J, Zhang TB, Li JS, Zhang J. Solidification characteristics of high Nb-containing γ -TiAl-based alloys with different aluminum contents. *Rare Met.* 2015;34(6):381.
- [5] Zollinger J, Gabalcova Z, Daloz D, Lapin J, Combeau H. Microsegregation induced microstructures in intermetallic Ti-46Al-8Nb alloy. *Kovove Mater.* 2008;46(5):291.
- [6] Kothari K, Radhakrishnan R, Wereley NM. Advances in gamma titanium aluminides and their manufacturing techniques. *Prog Aerosp Sci.* 2012;55:1.
- [7] Kim Y-W. Intermetallic alloys based on gamma titanium aluminide. *JOM.* 1989;41(7):24.
- [8] Zhang SZ, Zhang CJ, Du ZX, Hou ZP, Lin P, Chen YY. Microstructure and tensile properties of hot forged high Nb containing TiAl based alloy with initial near lamellar microstructure. *Mat Sci Eng A.* 2015;642:16.
- [9] Oehring M, Stark A, Paul JDH, Lippmann T, Pyczak F. Microstructural refinement of boron-containing beta-solidifying gamma-titanium aluminide alloys through heat treatments in the beta phase field. *Intermetallics.* 2013;32:12.
- [10] Hu D. Effect of boron addition on tensile ductility in lamellar TiAl alloys. *Intermetallics.* 2002;10(9):851.
- [11] Wang JN, Xie K. Grain size refinement of a TiAl alloy by rapid heat treatment. *Scripta Mater.* 2000;43(5):441.
- [12] Su MK, Zheng LJ, Lang ZB, Yan J, Zhang H. Microstructural evolution of a PM TiAl alloy during heat treatment in alpha plus gamma phase field. *Rare Met.* 2012;31(5):424.
- [13] Bauer J, Rogl P, Perrin A, Bohn M, Wolf W, Podlucky R, LeFricc Y, Antoine D. TiAl-based alloys with nickel. *Intermetallics.* 1996;4(1):71.
- [14] McKamey CG, Whang SH, Liu CT. Microstructural characterization of a γ -TiAl–Ni alloy produced by rapid solidification techniques. *Scr Metall Mater.* 1995;32(3):383.
- [15] Zhang J, Su X, Strom E, Zhong ZY, Li CH. Effects of minor addition of Ni on hot-deformation behavior of gamma TiAl alloy. *Mat Sci Eng A.* 2002;329:499.
- [16] Zhang J, Zhang Z, Su X, Zou D, Zhong Z, Li C. Microstructure preparation and hot-deformation of Ti–46.2Al–2.0V–1.0Cr–0.5Ni alloy. *Intermetallics.* 2000;8(4):321.
- [17] Schuster JC, Pan Z, Liu S, Weitzer F, Du Y. On the constitution of the ternary system Al–Ni–Ti. *Intermetallics.* 2007;15(9):1257.
- [18] Xia Y, Schaffer GB, Qian M. The effect of a small addition of nickel on the sintering, sintered microstructure, and mechanical properties of Ti–45Al–5Nb–0.2C–0.2B alloy. *J Alloy Compd.* 2013;578:195.
- [19] Raghavan V. Al–Ni–Ti (aluminum–nickel–titanium). *J Phase Equilib Diff.* 2010;31(1):55.
- [20] Han J, Xiao S, Tian J, Chen Y, Xu L, Wang X, Jia Y, Du Z, Cao S. Grain refinement by trace TiB₂ addition in conventional cast TiAl-based alloy. *Mater Charact.* 2015;106(8):112.
- [21] Overton JM. Thermophysical property and phase transformation determination of gamma-titanium aluminide intermetallics. Ottawa: Carleton University; 2006. 94.
- [22] Clemens H, Mayer S. Design, processing, microstructure, properties, and applications of advanced intermetallic TiAl alloys. *Adv Eng Mater.* 2013;15(4):191.
- [23] Schuster JC, Palm M. Reassessment of the binary aluminum–titanium phase diagram. *J Phase Equilib Diff.* 2006;27(3):255.
- [24] Shu S, Qiu F, Tong C, Shan X, Jiang Q. Effects of Fe, Co and Ni elements on the ductility of TiAl alloy. *J Alloy Compd.* 2014;617:302.